Separation and Purification Technology 253 (2020) 117510

Contents lists available at ScienceDirect

Separation and Purification Technology

journal homepage: www.elsevier.com/locate/seppur

Visible-light-induced activation of peroxymonosulfate by TiO_2 nano-tubes arrays for enhanced degradation of bisphenol A

Jialin Jia[a], Dongmei Liu[a,*], Songxue Wang[a], Huarui Li[a], Jiaxin Ni[a], Xiaobo Li[a], Jiayu Tian[b,*], Qiao Wang[c]

[a] State Key Laboratory of Urban Water Resource and Environment, Harbin Institute of Technology, Harbin 150090, China
[b] School of Civil Engineering and Transportation, Hebei University of Technology, Tianjin 300401, China
[c] School of Civil and Transportation Engineering, Guangdong University of Technology, Guangzhou 510006, China

ARTICLE INFO

Keywords:
TiO_2 nanotube arrays
Visible light
Peroxymonosulfate
PMS-TiO_2 complex
Bisphenol A

ABSTRACT

TiO_2 photocatalysis and peroxymonosulfate (PMS) oxidation can exhibit a good performance in ultraviolet light but a less activity in visible light (VL). Herein, the TiO_2 nano-tubes arrays (TiO_2NTAs) and PMS were combined to degrade bisphenol A (BPA) under VL irradiation. Surprisingly, about 94.6% of BPA was removed in TiO_2NTAs/PMS/VL system within 30 min, which was much higher than that of TiO_2NTAs/VL (20.1%) and PMS/VL (9.4%) systems. A series of spectroscopic characterizations and photoelectrochemical measurements confirmed the formation of PMS-TiO_2 complex with VL response, which can be excited by VL to transfer electrons to the conduction band (CB) of TiO_2 for activating PMS. The quenching tests and electron spin resonance (ESR) spectra indicated that $SO_4^{\cdot-}$ and ·OH were responsible for BPA degradation, and then the possible degradation pathways of BPA were proposed. Humic acid (HA) and chloride ions (Cl^-) significantly enhanced the BPA degradation, while bicarbonate (HCO_3^-) and phosphate ($H_2PO_4^-$) exhibited an inhibition effect. Moreover, TiO_2NTAs/PMS/VL system displayed an enhanced BPA degradation in tap water and drinking water compared with deionized water, and as an immobilization catalyst which fabricated on Ti plate, TiO_2NTAs exhibited excellent stability and separability without complex catalyst separation/recovery processes. We believe this work will provide a new insight of the VL-induced photocatalytic PMS activation in practical water treatment.

1. Introduction

Bisphenol A (BPA), as one of the most common endocrine disrupting compounds, has attracted a great concern owing to its potential threat to human and ecosystems [1]. Due to the extensive use, BPA has frequently been detected in water environment. It has been found that the concentrations of BPA were 1.47 μg/L in groundwater [2], 56 μg/L in surface water [3] and 370 μg/L in wastewater treatment plants (WWTPs) effluents [4]. Conventional treatments, such as adsorption [5], filtration [6] and biodegradation [7], have been proved difficult to remove BPA effectively. Thus, an effective method for BPA removal is urgently needed.

Advanced oxidation processes (AOPs) have been intensively used to remove organic pollutants due to the production of various reactive oxygen species (ROS). Among various AOPs, sulfate radical-based AOPs (SR-AOPs) which represent by peroxymonosulfate (PMS) or peroxydisulfate (PDS) has drawn enormous interests thanks to their good chemical stability and the formation of high reactive species (e.g. $SO_4^{\cdot-}$ and ·OH) [8]. Various techniques have been developed to activate PMS for degradation of pollutants, such as ultrasound [9], ultraviolet [10], heat [11], and electrochemistry [12]. Besides, various materials and materials-based AOPs were also used to induce PMS activation [13,14,15]. However, these methods either require abundant energy input or the powder catalyst is difficult to be separated and recycled, and may bring the secondary pollution. Thus, economic and environmental friendly activation techniques are still highly in demand.

Due to accounting for approximate 45% of the solar spectrum, the visible light (VL) induced PMS activation is much desirable and promising compared with ultraviolet activation (only accounting for about 4% of the solar spectrum). Some photocatalysts such as TiO_2 [16], $BiVO_4$ [17], CeO_2/Co_3O_4 and $ZnFe_2O_4$ [18] have been developed for PMS activation under VL irradiation. Among these catalysts, TiO_2 has been considered as the most promising semiconductor of photocatalysis because of its nontoxicity, low cost and long-term photostability [19], and TiO_2 photocatalysis has been reported to effectively activate PMS for organic pollutants removal [20,21,22,23]. Particularly, Chen et al.

* Corresponding authors.
E-mail addresses: ldm819@126.com (D. Liu), tjy800112@163.com (J. Tian).

https://doi.org/10.1016/j.seppur.2020.117510
Received 28 February 2020; Received in revised form 17 July 2020; Accepted 30 July 2020
Available online 03 August 2020

[22] reported that the main activation mechanism for the enhanced removal of Acid Orange 7 in the TiO_2/PMS/VL system was that the VL irradiated Acid Orange 7 photosensitization to produce electrons for activating PMS into ·OH and $SO_4^{\bullet -}$. The results indicated that a notable synergistic effect was observed in the TiO_2/PMS/VL system. Besides the PMS, TiO_2 can also activate another peroxide H_2O_2 through metal–ligand charge transfer mechanism under VL irradiation. In this process, H_2O_2 can combine with TiO_2 to generate a VL-responsive complex (> Ti-OOH), which is derived from the complexing of the hydroxyl component on the surface of Ti with H_2O_2 and releasing a H_2O molecule (> Ti-OH + H_2O_2→ > Ti-OOH + H_2O). Under VL irradiation, the Ti-OOH complex can be excited and transfer the electrons to the conduction band (CB) of TiO_2. Then, the excited electron reductively splits H_2O_2 into ·OH, and the surface-complexed intermediate Ti-·OOH further releases $1/2O_2$ and converted into initial > Ti-OH for next reaction [23]. Considering the VL-responsive character of H_2O_2-complexed TiO_2, PMS activation by VL-induced photocatalysis may also follow the similar activation mechanism. That is, PMS not only acts as a radical precursor metal–ligand to complex the photocatalyst, but also a metal–ligand to complex the photocatalyst when combined PMS and TiO_2 under VL irradiation.

In this work, the TiO_2 nano-tubes arrays (TiO_2NTAs) was selected to investigate the formation of metal–ligand (PMS-TiO_2) complexation and its performance of photocatalytic activation PMS under VL irradiation. The aim of selection of the immobilized TiO_2NTAs was to solve the secondary pollution and tedious recycle of the pulverous catalyst in the suspending system. The complexation of PMS with TiO_2 and the charge transfer were confirmed by a series of spectroscopic characterizations. The VL response of PMS-TiO_2 complex was verified by the UV–vis diffuse reflectance spectra (DRS), and the PMS activation was confirmed by cyclic voltammetry (CV) curves. The ROS involved in the reaction system were identified via the quenching experiments and instrument characterization, and the probable degradation pathways of BPA were proposed. Besides, the effects of operating parameters and water matrices on BPA degradation were investigated, and the performance of the system applied in tap water and drinking water was explored. Finally, the stability and reusability of TiO_2NTAs were also evaluated.

2. Experimental section

2.1. Materials

Titanium plates (0.5 mm thickness, 99.5% purity) were obtained from Shenzhen Futai metal materials Co. Ltd., China. Peroxymonosulfate (PMS, $KHSO_5$·0.5$KSHSO_4$·0.5K_2SO_4) and 5,5-dimethyl-1-pyrolin-Noxide (DMPO) were obtained from Sigma-Aldrich Co. Ltd., USA. Bisphenol A (BPA), tert butyl alcohol (TBA), methanol (MeOH) and humic acid (HA) were purchased from Aladdin Chemistry Co. Ltd., China. HA was refined according to the previous literature [24]. All other reagents were of analytical grade. Deionized water was employed throughout the experiments.

2.2. Preparation of TiO_2NTAs

The TiO_2NTAs were fabricated by anodization of Ti plates in an aqueous solution which containing 0.5 wt% NH_4F in glycerol including a 40% (v/v) of deionized water. Before anodization, Ti plates were pretreated according to the previous literature [25]. Afterwards, the anodization was conducted in a two-electrode system, in which the as-treated Ti plate was set as anode and Pt plate as cathode. The anodization process was carried out under a constant 20 V for 2 h at 25 °C, with the distance between the two electrodes set at 2 cm. The obtained TiO_2NTAs samples were rinsed with deionized water for several times, and then were dried at 70 °C for 4 h. Finally, TiO_2NTAs with anatase phase was obtained by annealing in a tube furnace at 500 °C for 2 h with a ramping rate of 3 °C/min.

2.3. Characterization

The morphology of the prepared TiO_2NTAs and electron energy loss spectroscopy (EELS) mapping were observed using a field emission scanning electron microscope (FE-SEM, Hitachi SU8010). The crystal phase of the sample was confirmed with the Bruker D8 X-ray diffractometer equipped with Cu Ka radiation (λ = 0.15418 nm). The surface composition, the distribution of sulfur and the surface functional groups of the materials were recorded on a X-ray photoelectron spectroscopy (XPS, ESCALAB 250, VG Scientific) with Al Kα line (1486.6 eV) as an excitation source. The reactive radicals were identified by using Electron spin resonance (ESR) spectroscopy (Bruker A300 spectrometer, Germany). The UV–vis diffuse reflectance spectra (DRS) were collected by conducting a spectrophotometer (Shimadzu, UV2550). Fourier transform infrared spectroscopy (FT-IR) was tested with a Perkin Elmer Spectrum One instrument.

2.4. Photoelectrochemical measurement

All the photoelectrochemical measurements including transient photocurrent response (TPR), electrochemical impedance spectroscopy (EIS) and cyclic voltammetry (CV) were conducted with an electrochemical station (Metrohm PARSTAT302A, Switzerland). A typical three-electrode system was employed, in which the TiO_2NTAs, Pt electrode and saturated calomel electrode (SCE) were employed as the work electrode, counter electrode and reference electrode, respectively. The supporting electrolyte was 0.1 M Na_2SO_4 solution. The EIS was measured with a frequency range of 0.01 Hz ~ 100 KHz. The applied voltages of CV measurement ranged from −1.5 to 0.6 V at a scan rate of 50 mV s^{-1}.

2.5. BPA degradation

Photocatalytic activation of PMS for BPA (1 mg/L) degradation was conducted in a 100 mL beaker which contained 50 mL aqueous solution of BPA under magnetic stirring. The VL source was obtained by a 300 W Xenon lamp (Beijing NBeT) with a 400 nm cut-off filter. The distance between the solution interface and the light was set as 10 cm. Prior to irradiation, the prepared TiO_2NTAs was fixed in the beaker with the photoreaction areas of 1 × 2 cm^2. Afterwards, PMS was added into the reactor with/without of substrates (e.g., Cl^-, NOM) to trigger the reaction with Xenon lamp switched on (Fig. S1). The pH of the reaction solution was 3.98 after the addition of PMS to system. In addition, during the study of pH influence, 1.0 M H_2SO_4 or NaOH solution were employed to control the pH of the reaction system. The temperature was maintained at 25 ± 2℃ by continuous circulation cooling water. At given time intervals, 1.0 mL of reaction solution was withdrawn and filtered through a 0.22 μm membrane, and was then injected into a brown vial with 0.5 mL methanol (MeOH) inside to terminate the oxidation. Most experiments were conducted in triplicate, the average values were employed with standard deviations which represented by error bars.

2.6. Analytical methods

The BPA concentration was measured by the UPLC system (Waters, MA, USA) with a BEH C18 column (1.0 × 50 mm, 1.7 μm) and an UV detector (λ = 230 nm). The mobile phase consisted of 65% MeOH and 35% ultrapure water with a flow rate of 0.1 mL/min. The intermediate products of BPA oxidation were detected by employing HPLC/ESI-QQQ (5500 MS, ABSciex USA). The mass spectra was measured with a scan range of 50–600 *m/z* in a negative mode. The ion spray voltage was 4500 V, the source temperature was 500℃, the curtain gas and nebulizer gas were 35 psi and 50 psi, respectively. The de-clustering

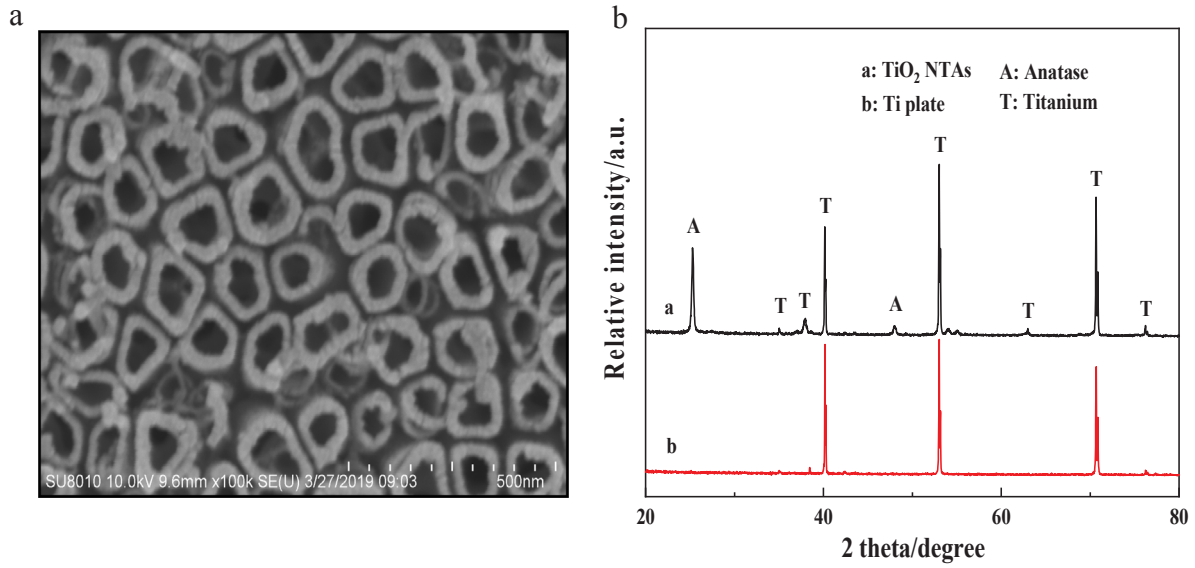

Fig. 1. SEM images (a) and X-ray diffraction (XRD) pattern (b) of TiO_2NTAs.

potential (DP) was 100 V, and the collision energy (CE) was −30–45 V.

3. Results and discussion

3.1. Characterization of the TiO_2NTAs

Fig. 1a presents the surface morphology (SEM image) of the prepared TiO2NTAs. The highly ordered nano-tubular structure could be clearly observed with an average inner diameter of 100 nm and the wall thickness of 20 nm. Fig. 1b exhibits the XRD patterns of the Ti plate and the prepared TiO2NTAs. Both of them showed obvious titanium matrix diffraction peaks (JCPDS NO. 44-1294). In addition, the TiO2NTAs showed obvious anatase diffraction peaks at 25.3° and 48.1°, which demonstrated that anatase TiO_2NTAs were successfully prepared.

3.2. Removal of BPA by TiO_2NTAs/PMS/VL system

The BPA degradation under different conditions were explored, and the results were presented in Fig. 2a. Clearly, the BPA degradation in VL was negligible without TiO_2NTAs and PMS (blank group). The addition of PMS resulted in only 9.4% removal of BPA within 30 min under VL irradiation. The similar result was also got by Liu et al., who also found that VL activated PMS could degrade organic pollutant to some extent [26]. In addition, after 30 min of reaction, around 20.1% of BPA was removed in the TiO_2NTAs/VL system. The BPA removal was likely similar to that the degradation of phenolic compounds in the TiO_2/VL photocatalytic system [27]. The generation of surface complexes of BPA on TiO_2NTAs surface are active to VL, and could be excited by VL to transfer electrons to the CB of TiO_2. Then the electrons could react with dissolved oxygen to produce the active oxidants for subsequent oxidation of organic pollutants. Surprisingly, when PMS was added into the TiO_2NTAs/VL system, the BPA degradation efficiency improved significantly. About 94.6% of BPA was oxidized within 30 min, which was 4.7 and 10.1 times higher than that of TiO_2 NTAs/VL and PMS/VL systems, respectively. Besides, the BPA degradation followed well pseudo-first-order kinetics, and the reaction rate constant of the TiO_2

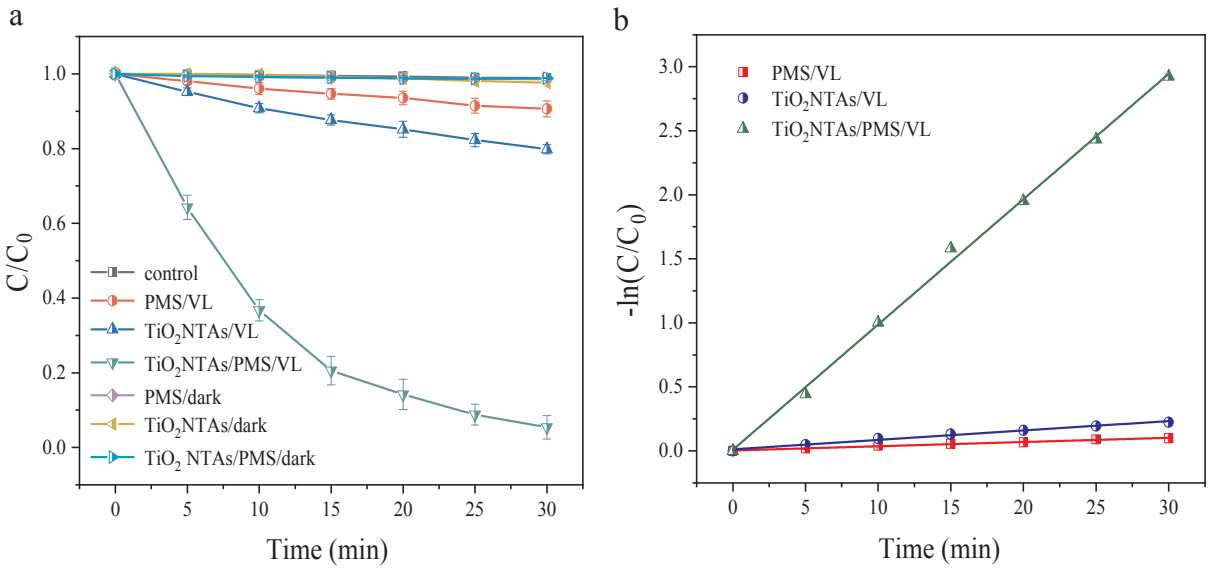

Fig. 2. BPA degradation under different systems (a), kinetics liner fitting curves (b). Experimental conditions: [PMS] = 0.05 mM, [BPA] = 1 mg/L, [pH] = 3.98, T = 25℃.

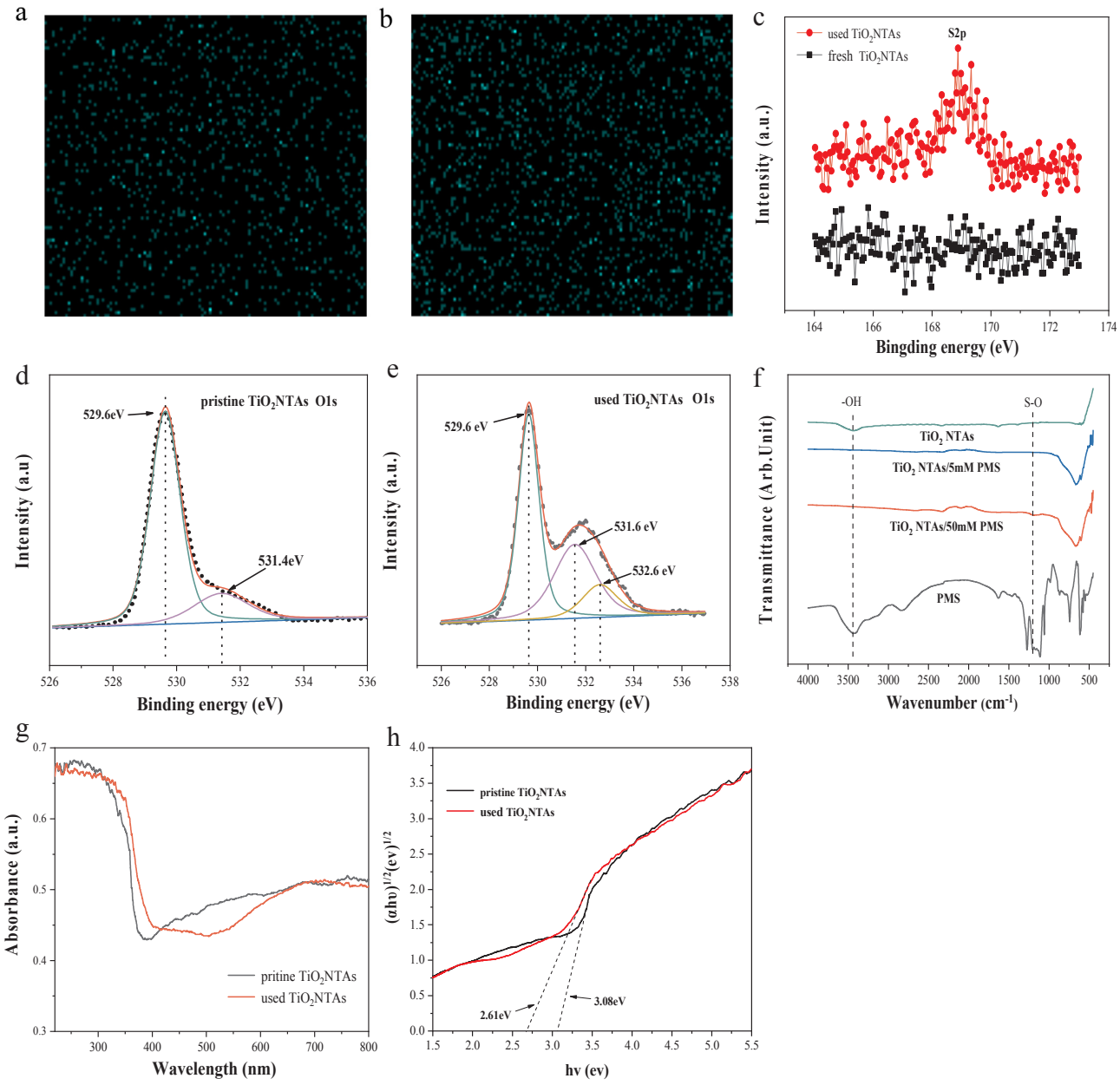

Fig. 3. EELS elemental mapping image of S in the pristine (a) and used TiO_2NTAs (b), the high resolution XPS spectra of S2p of pristine and used TiO_2NTAs (c), the high resolution XPS spectra of O1s of pristine (d) and used (e) TiO_2NTAs, FT-IR spectra (f), UV–vis diffuse reflection spectra (g) and $(ahv)^{1/2}$-hv relation curve of pristine and used TiO_2NTAs.

NTAs/PMS/VL system (k = 0.098 min^{-1}) was calculated to be 13.2 and 29.7 times higher than those of TiO_2 NTAs/VL (k = 0.0074 min^{-1}) and PMS/VL (k = 0.0033 min^{-1}) systems, respectively (Fig. 2b), indicating that a synergistic effect for the degradation of BPA was occurred when combining TiO_2NTAs and PMS under VL irradiation.

3.3. Formation of PMS-TiO_2 complex

Fig. 3a and b present the EELS maps of the sulfur element in TiO_2NTAs before and after reaction in the TiO_2NTAs/PMS/VL system. Compared with the pristine TiO_2NTAs, the used TiO_2NTAs exhibited an increase in the content of sulfur element (sulfur element in the pristine TiO_2NTAs may be ascribed to the impurities on the surface of TiO_2NTAs or the error bring by the instrument), which indicated the formation of surface sulfur species on the surface of TiO_2NTAs. Besides, the S2p high-resolution XPS spectra of the pristine and used TiO_2NTAs in PMS solution were investigated (Fig. 3c). The S2p peak with the binding energy of 168.8 eV was observed only in the used TiO_2NTAs, confirming the existence of surface sulfur species [28]. Meanwhile, the O1s XPS spectra of the pristine and used TiO_2NTAs were fitted to two (529.6 eV and 531.4 eV) and three (529.6 eV, 531.6 eV and 532.6 eV) kinds of chemical states, respectively (Fig. 3d and e). The corresponding XPS data were listed in Table 1. The binding energy at ca.529.6 eV and 531.4 eV could be attributed to the lattice oxygen in TiO_2 and hydroxyl groups/oxygen in sulfate, respectively [29]. While the peak at ca.532.6 eV could be assigned to oxygen of H_2O adsorbed on TiO_2 [30]. Obviously, the content of hydroxyl groups/oxygen in sulfate of the used TiO_2NTAs was higher than that of pristine TiO_2NTAs, indicating that a sulfur-oxygen species existed on the surface of TiO_2. The S-O bond stretching of the used TiO_2NTAs was observed at 1199 cm^{-1} in the FT-IR spectra [31], and became more evident when 10-fold higher PMS dose was added to the TiO_2NTAs/VL system (Fig. 3f), suggesting the

Table 1
Curve fitting results of high resolution XPS spectra for the O1s region.

Sample		Lattice oxygen	Sulfate oxygen/ hydroxyl oxygen	H_2O oxygen
Pristine TiO_2NTAs	r (%)	80.23	19.76	
	Eb (eV)	529.6	531.4	
Used TiO_2NTAs	r (%)	50.27	36.21	13.51
	Eb (eV)	529.6	531.6	532.6

probably linkage of PMS to the surface of TiO_2NTAs. In addition, the stretching vibrations of O–H bond of PMS and TiO_2 at around 3400 cm^{-1} were disappeared after the combination of them, further indicating that a condensation reaction was occurred.

The UV–vis diffuse reflectance spectra (UV–vis DRS) and the corresponding $(\alpha h\upsilon)^{1/2}$-$h\upsilon$ relation curve of the pristine and used TiO_2NTAs were shown in Fig. 3g and h, respectively. As can be seen, the absorption edge of the used TiO_2NTAs displayed a distinct red-shifting compared to the pristine TiO_2NTAs. Furthermore, according to Kubelka-Munk equation $(\alpha h\upsilon)^2 = k(h\upsilon\text{-}Eg)$ (where, α is absorption coefficient, h Planck constant, υ light frequency, Eg band energy), the band gap energies of the pristine TiO_2NTAs and used TiO_2NTAs were calculated to be 3.08 eV and 2.61 eV, respectively, indicating that the addition of PMS could induce the formation of VL-responsive PMS-TiO_2 complex.

3.4. Charge transfer of PMS-TiO_2 complex under VL irradiation

Similar to H_2O_2-TiO_2 complex, the direct electron transfer from the PMS-TiO_2 complex to the CB of TiO_2 might also occur when under VL irradiation. The transferred electron might activate PMS to generate the corresponding radicals. To confirm the electron transfer of PMS-TiO_2 complex under VL irradiation, a series of photoelectrochemical characterizations were measured. Fig. 4a depicts the transient photocurrent of TiO_2NTAs in different systems. As can be seen, neither TiO_2NTAs nor TiO_2NTAs/PMS showed photocurrent response in the dark. However, as the Xenon lamp was switched on, the photocurrent was observed in both systems. The pristine TiO_2NTAs induced a weak photocurrent response, which could be ascribed to its wide band gap with a very little VL absorption. Noticeably, the TiO_2NTAs/PMS system exhibited a significant photocurrent generation in contrast with TiO_2NTAs alone. The photocurrent results could be taken as an evidence of the direct charge transfer from the PMS-TiO_2 complex to the CB of TiO_2 [28]. Furthermore, the EIS measurements of different reaction systems were compared to support the photocurrent results (Fig. 4b). Normally, the smaller circular arc radius in the plots of EIS Nyquist manifested the better charge transfer ability [32]. Obviously, the circular arc diameter was decreased with VL irradiation, which could be attributed to the effective charge transfer under VL irradiation. Compared with TiO_2NTAs/VL system, TiO_2NTAs/PMS/VL system exhibited a smaller arc diameter, indicating that the electron transfer in the PMS/TiO_2NTAs/VL system was faster than the TiO_2NTAs/VL system. This further confirmed the directly electron transfer from the PMS-TiO_2 complex to the CB of TiO_2.

In addition, as can be seen in Fig. 4c, the curve shape of TiO_2NTAs/dark system was similar to those of TiO_2NTAs/PMS/dark and TiO_2NTAs/VL systems. All of the three systems presented a small reduction peak from −1.0 V to −1.2 V, which could be ascribed to a common reduction for TiO_2NTAs electrode [33]. While a pronounced reduction peak at −0.62 V appeared in the TiO_2NTAs/PMS/VL system, indicating that a reduction reaction was occurred in the system. This might be attributed to the fact that PMS could be activated by the transferred electrons which mainly derived from the PMS-TiO_2 complex and a small part from TiO_2NTAs under VL excitation. In this process, some PMS bonded to the TiO_2 surface could serve as the electron donors, while the other PMS acted as the electron acceptors might be activated into radicals.

3.5. Catalytic oxidation mechanism

The radical quenching experiments were carried out to identify the reactive species produced in the TiO_2NTAs/PMS/VL system (Fig. 5a). The ·OH and $SO_4^{\bullet-}$ are generally considered as the common reactive species for pollutant degradation in PMS oxidation processes. They are usually distinguished by TBA and MeOH since they own different rate constants to the two radicals (TBA: 3.8–7.6 × 10^8 $M^{-1}s^{-1}$ for ·OH, MeOH: 1.6–7.7 × 10^7 M^{-1} s^{-1} for ·OH and 1.2–2.8 × 10^9 M^{-1} s^{-1} for $SO_4^{\bullet-}$) [34,35]. In Fig. 5a, the degradation rate of BPA was reduced by 58.59% and 47.1% within 30 min when MeOH and TBA were added in the reaction system, respectively. Hence, it could be deduced that $SO_4^{\bullet-}$ and ·OH were both responsible for the oxidation of BPA. It was worth noting that the degradation of BPA was not completely suppressed when the excess MeOH was added, the removal efficiency of BPA was 36.0% (94.6%-58.6%), even minus the removal efficiency caused by TiO_2NTAs (20.1%), the degradation rate could still reach 15.9%. The similar phenomenon was also found by Jo et al. [28]. For this, our speculation is that the PMS-TiO_2 complex itself may have the ability to oxidize pollutants directly. However, so far we have not found an effective way to prove this hypothesis. Since it was a very interesting and meaningful issue to be solved, we will try to explore it in our future work.

Besides, the ESR measurements were conducted to further confirm the radicals by employing DMPO as a trapping agent. As shown in Fig. 5b, there were no definable characteristic peaks found in the TiO_2NTAs/PMS/Dark system. While the characteristic peaks of DMPO-

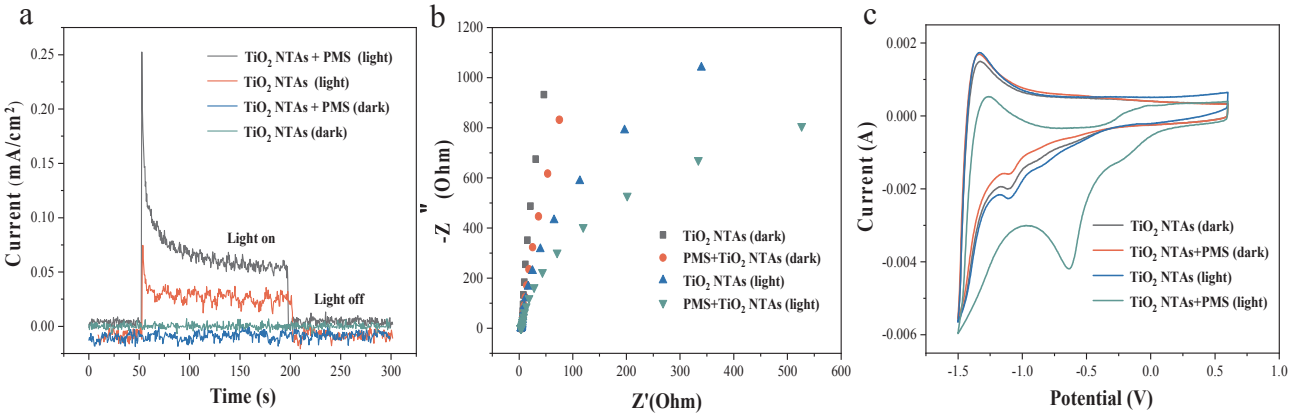

Fig. 4. Photocurrent generation (a), EIS Nyquist plots (b), and CV curves (c) of TiO_2NTAs in the absence and presence of PMS in dark and VL irradiation.

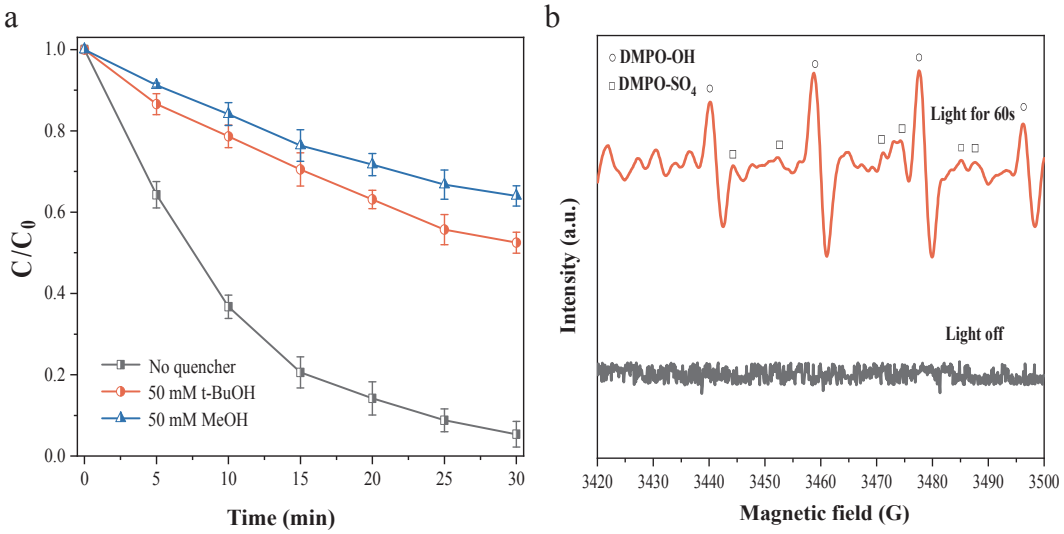

Fig. 5. Effects of quenchers on the activity of TiO_2NTAs/PMS/VL system for BPA degradation (a) and ESR spectra trapped by DMPO in TiO_2NTAs/PMS/Dark and TiO_2NTAs/PMS/VL systems (b).

$SO_4^{\bullet-}$ adduct (α_N = 13.2 G, α_H = 9.6 G, α_H = 1.48 G and α_H = 0.78 G) and DMPO-·OH adduct (aN = aH = 14.9 G) with the typical quartet lines with peak strength of 1:2:2:1 were emerged in the TiO_2NTAs/PMS/VL system [36]. The ESR tests further confirmed the existence of $SO_4^{\bullet-}$ and ·OH radicals in the TiO_2NTAs/PMS/VL system.

Combining the above results and analyses, a possible mechanism for enhanced BPA degradation by the TiO_2NTAs/PMS/VL system was proposed in Fig. 6. On one hand, PMS was likely to participate in the formation of PMS-TiO_2 complex at TiO_2NTAs surface, and thus the electrons would be transferred from PMS-TiO_2 complex to the CB of TiO_2 under VL irradiation as described in section 3.3 and 3.4 (Eq. (1) and (2)). As an electron acceptor, another portion of PMS would combine with these electrons to produce $SO_4^{\bullet-}$ (Eqs. (3)), and the generated $SO_4^{\bullet-}$ could further react with H_2O to generate ·OH (Eqs. (4)). On the other hand, the complexation of BPA on TiO_2NTAs surface might offer another electron transfer pathway for PMS activation (Eqs. (5) and (6)) to generate $SO_4^{\bullet-}$ and ·OH. The residual $\bullet SO_5^-$ could be combined to form $SO_4^{\bullet-}$, and TiO_2 could adsorb the –OH for next cycle (Eqs. (7) and (8)). All the generated reactive species resulted in the degradation of BPA in the TiO_2NTAs/PMS/VL system (Eq. (9)).

Based on previous study, the ratio of reaction rate constants could represent the degradation contribution of different processes [37]. In this study, the degradation rate constant of BPA by the PMS-TiO_2 complex system accounted for 89.1% ((0.098 min^{-1} (TiO_2NTAs/PMS/VL)-0.0074 min^{-1} (TiO_2NTAs/VL)-0.0033 min^{-1} (PMS/VL)/0.098 min^{-1}) of the total BPA degradation, indicating that electrons transfer of PMS-TiO_2 complex under VL irradiation played a dominant role in the activation of PMS for organic pollutant oxidation.

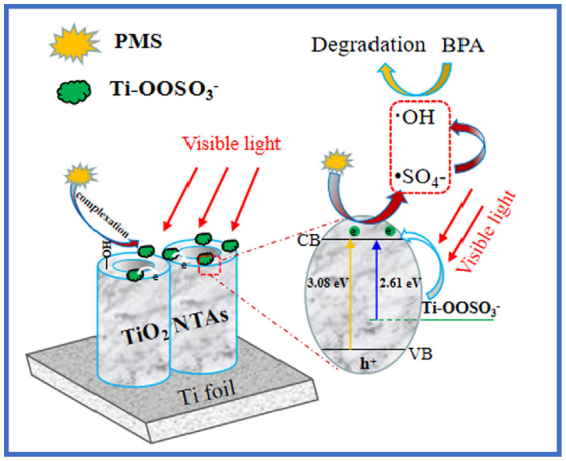

Fig. 6. Proposed mechanism of PMS activation by TiO_2NTAs under VL. irradiation.

$$Ti\text{-}OH + HSO_5^- \rightarrow Ti\text{-}OOSO_3^- + H_2O \quad (1)$$

$$Ti\text{-}OOSO_3^- + h\nu \rightarrow Ti\text{-}{\cdot}OOSO_3 + TiO_2\,(e^-) \quad (2)$$

$$TiO_2\,(e^-) + HSO_5^- \rightarrow SO_4^{\bullet-} + OH^- \quad (3)$$

$$SO_4^{\bullet-} + H_2O \rightarrow H^+ + SO_4^{2-} + {\cdot}OH \quad (4)$$

$$TiO_2\text{NTAs-BPA} + h\nu \rightarrow TiO_2\text{NTAs-BPA}^* + e^- \quad (5)$$

$$e^- + HSO_5^- \rightarrow SO_4^{\bullet-} + {\cdot}OH \quad (6)$$

$$Ti\text{-}{\cdot}OOSO_3 + Ti\text{-}OOSO_3 \rightarrow 2SO_4^{\bullet-} + 2Ti \quad (7)$$

$$TiO_2 + {-}OH \rightarrow TiO_2\text{-}OH \quad (8)$$

$$SO_4^{\bullet-}/{\cdot}OH + BPA \rightarrow Products \quad (9)$$

In addition, to fully understand the oxidation process of BPA in the TiO_2NTAs/PMS/VL system, the oxidation intermediates of BPA were identified by LC-MS/MS analysis. Based on the LC-MS/MS results and previous reports [38,39,40,41], the possible intermediates were listed in Fig. S2 and Table S1, and the probable degradation pathways of BPA were proposed in Fig. 7. Firstly, the C–O bond of BPA might be attacked by sulfate radicals or hydroxyl radicals via a dehydroxylation pathway, generating C1 (4-Cumylphenol, m/z = 211). Secondly, the reactive species continue to attack the electron-rich alkyl carbon leading to the formation of C2 (2-(4-hydroxypheny)-propanol-2-ol, m/z = 151). In addition, BPA might also be hydroxylated by hydroxyl radicals to convert to C3 (BPA-o-catechol, m/z = 243), which could be transformed into C4 (Quinone of BPA-o-catechol, m/z = 241), and further oxidized into C2. Then, the tertiary hydroxyl would be attacked, resulting in the formation of C5 (4-Hydroxyacetophenone, m/z = 135). Besides, the aromatic ring of C3 might be attacked to form C6 (dihydroxylated BPA, m/z = 259). Finally, the ring-opening reactions might occur on C5 and C6 in the presence of sulfate radicals and hydroxyl radicals, which would be transformed into C7 (divinyloxyethane, m/z = 113) and further be mineralized to CO_2 and H_2O.

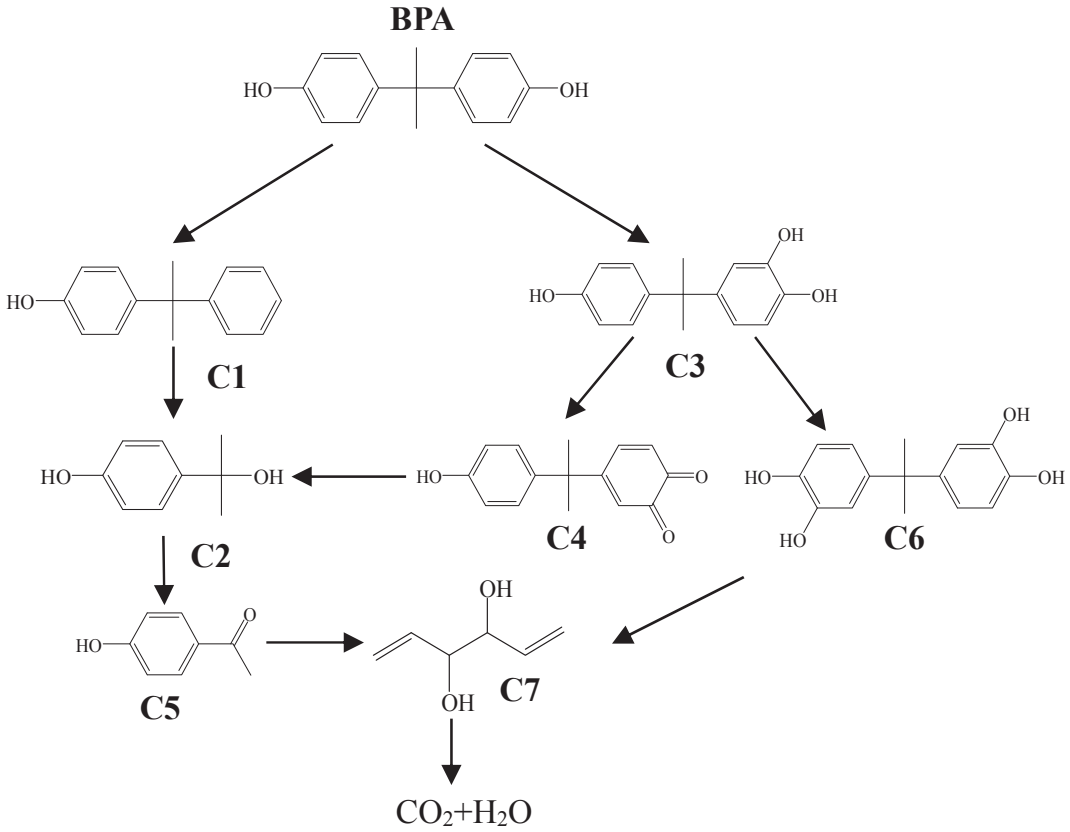

Fig. 7. Probable degradation pathways of BPA in TiO_2NTAs/PMS/VL system.

3.6. Effects of reaction parameters

Fig. 8a presents the effect of reaction areas of TiO_2NTAs on BPA degradation in the TiO_2NTAs/PMS/VL system (the dark adsorption was shown in Fig. S3a). As shown in Fig. 8a, the removal efficiency of BPA promoted from 46.7% to nearly 100% with the reaction area of TiO_2NTAs increased from 0.5 to 8 cm^2 within 30 min. Generally, the greater reaction areas could provide more reactive sites, which was beneficial to produce more reactive species to degrade BPA. Nevertheless, when the reaction area was enlarged from 4 to 8 cm^2, the increase in degradation rate was not significant. This could be explained by that the PMS dose was fined in the system, though the reaction area of TiO_2NTAs increased, there was no enough PMS to react with it to form the corresponding reactive species, thus there is a little difference in the amount of reactive species between the 8 and 4 cm^2 groups, resulting in the insignificant improvement of removal efficiency.

Fig. 8b depicts the effect of PMS dose on BPA degradation (the dark adsorption was shown in Fig. S3b) in the TiO_2NTAs/PMS/VL system. As can be seen, the removal efficiency of BPA was promoted as the concentration of PMS increased from 0.03 (59.4%) to 0.07 mM (97.3%). This could be attributed to that the higher PMS dose would lead to the more generation of active radicals, resulting in the enhancement of BPA degradation [42]. However, with PMS concentration further increased, the degradation showed a declining trend, which decreased from 97.3% (0.07 mM) to 77.2% (0.5 mM). Although increasing PMS content enhanced the reactive radicals concentration, the excessive PMS could react with the $SO_4^{\bullet -}$ to generate a less reactive radical ($SO_5^{\bullet -}$) (Eq. (10)) [43]. Moreover, the reaction between $SO_4^{\bullet -}$ and ·OH (Eq. (11)) and the self-scavenging of $SO_4^{\bullet -}$ radicals (Eq. (12)) [44] also decreased the concentration of reactive radicals, thus retarding the degradation of BPA.

$$HSO_5^- + SO_4^{\bullet -} \rightarrow SO_5^{\bullet -} + SO_4^{2-} + H^+ \quad (10)$$

$$SO_4^{\bullet -} + \cdot OH \rightarrow HSO_5^- \quad (11)$$

$$SO_4^{\bullet -} + SO_4^{\bullet -} \rightarrow S_2O_8^{2-} \quad (12)$$

The effect of initial solution pH ranging from 3.0 to 11.0 on BPA degradation in the TiO_2NTAs/PMS/VL system was also tested. As shown in Fig. 8c. The pH value of 3.98 was the natural pH of the system. Interestingly, it was found that the BPA degradation increased when the system was set to be more acidic or alkaline condition, and the acidic condition was more conducive to BPA degradation. This could be ascribed to that under acidic and alkaline conditions, the surface of TiO_2NTAs is positively and negatively charged, respectively (the pH of the point of zero charge is 6.3) [45], and PMS exists in the form of anion in a wide pH range (i.e., pKa1 = 0.4 and pKa2 = 9.3) [46]. Due to the electrostatic attraction between PMS and TiO_2NTAs at acidic condition, more PMS could be adsorbed on the surface of TiO_2NTAs. This could enhance the possibility of the PMS-TiO_2 complex formation and the reaction between PMS and electrons which derived from the PMS-TiO_2 complex under VL irradiation, thus favoring BPA degradation. In reverse, because of the electrostatic repulsion between TiO_2 and PMS under alkaline condition, PMS has less opportunity to accumulate on the surface of TiO_2 in quantity, this would greatly reduce the formation of PMS-TiO_2 complex and the chance of reaction between electrons and PMS, hence leading to the decrease in BPA degradation. However, it was also reported that the alkaline condition could facilitate the activation of persulfate, where the negatively charged –OH was more likely to donate the electron compared with H_2O molecules [47]. The results of the dark adsorption also confirmed this (Fig. S3c). Thus, in this way, the BPA degradation was enhanced with the pH of the system increased from 7.0 to 11.0.

The influence of initial BPA concentration on BPA removal in the TiO_2NTAs/PMS/VL system was presented in Fig. 8d (the dark adsorption was shown in Fig. S3d). As can be seen, the BPA removal percentage within 30 min was gradually decreased from 94.6% to 8.9% as

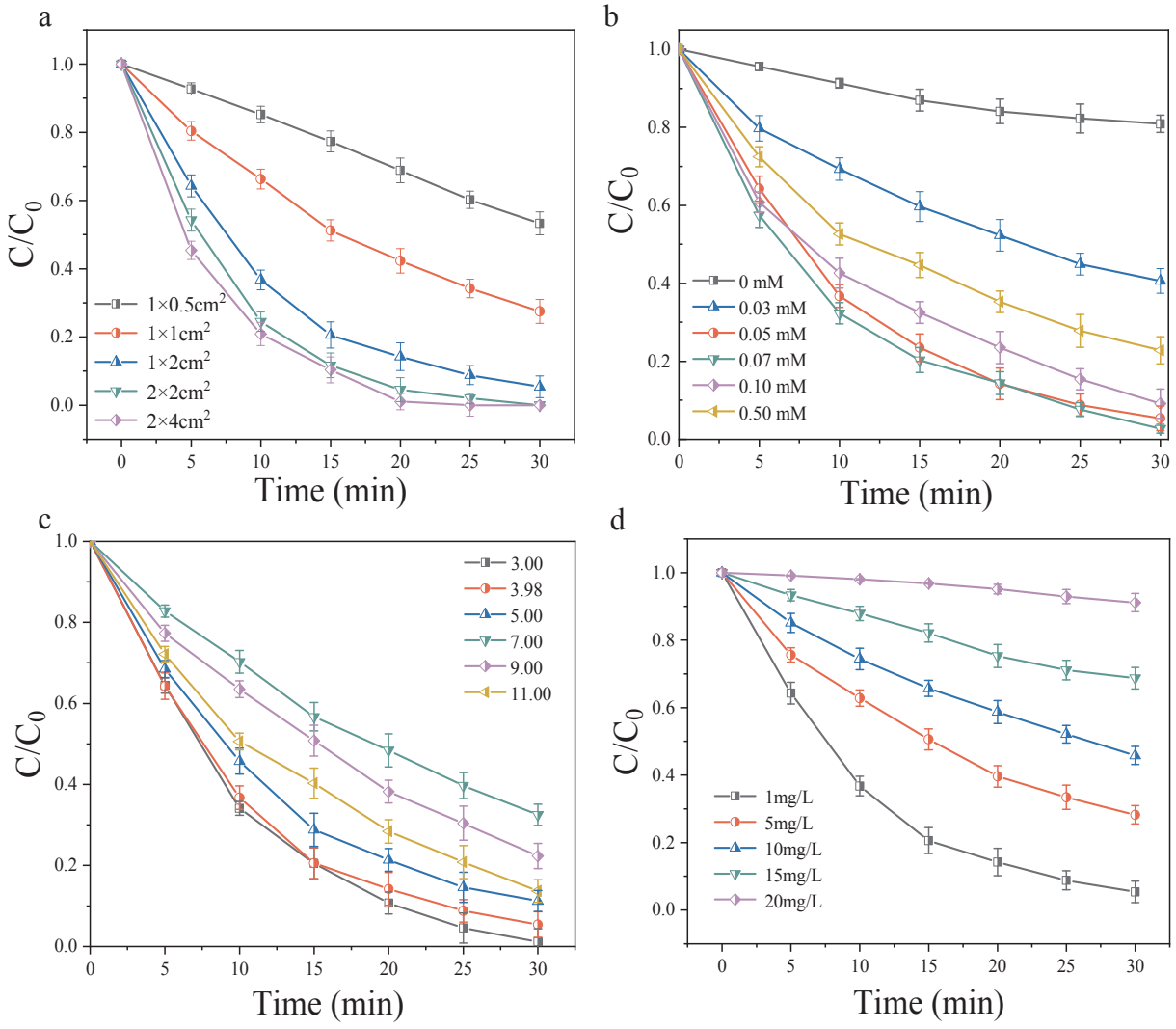

Fig. 8. Influence of reaction parameters on BPA degradation in the TiO_2NTAs/PMS/VL system: reaction areas of TiO_2NTAs (a), initial PMS concentration (b), initial pH value (c), and initial BPA concentration (d). Experimental conditions: [BPA] = 1–20 mg/L, [PMS] = 0–0.5 mM, [reaction areas of TiO_2NTAs] = 0.5–8 cm^2, [pH] = 3–11, T = 25℃.

the initial BPA concentration increased from 1 to 20 mg/L. Theoretically, the overall ROS yield would be not increased once the PMS dose was fined under the identical condition. Hence, the removal percentages of BPA were relatively low at high BPA concentrations in a specific reaction time. However, as the previous study reported, it was difficult to analyze the influence of initial organic pollutant concentration based on the temporal evolution of normalized concentration [48]. Thus, the initial rate was employed as a better method to study this issue. As shown in Fig. S4, the initial rate of BPA was not linearly corresponding to the initial BPA concentration, and too low (1 mg/L) or too high (20 mg/L) concentration of BPA has a relatively small initial rate. This could be explained by that the increased BPA concentration can improve the opportunity of collision between reactive species and BPA, thus leading to an accelerated reaction. While the excess BPA might occupy the reactive sites of TiO_2 nano-tubes and inhibit the PMS adsorption on it, hindering the generation of reactive species and thus resulting in a slow rate of reaction.

3.7. Effect of water matrices on BPA degradation

There are various inorganic anions in natural water bodies such as Cl^-, HCO_3^-, $H_2PO_4^-$, NO_3^- and SO_4^{2-}, which would influence free radical-induced reactions in water treatment process [49,50]. In this work, three common inorganic anions, namely Cl^-, HCO_3^- and $H_2PO_4^-$ were chosen to evaluate the effect of inorganic anions on BPA degradation. Besides, as one of the representative constitutes of NOM, the influence of humic acid (HA) on BPA degradation was also investigated.

Fig. 9a depicts the BPA degradation behavior at different Cl^- concentrations ranging from 0 to 5 mM. With the presence of Cl^-, the removal efficiency of BPA was obviously promoted. It has been reported that as an effective scavenger for $SO_4^{\bullet-}$ and ·OH, Cl^- could rapidly react with $SO_4^{\bullet-}$ and ·OH to produce some active chlorine species including Cl·, $\cdot Cl_2^-$, $ClOH^{\bullet-}$, and Cl_2/HOCl, which promoting the BPA degradation. In addition, PMS can directly react with Cl^- to form HOCl and Cl_2 [51,52]. Thus, it was likely that the reactive chlorine species promoted the BPA degradation.

Unlike the Cl^-, the addition of bicarbonate distinctly suppressed the BPA degradation. As shown in Fig. 9b, the degradation rate of BPA decreased from 94.6% to 51.9% within 30 min with HCO_3^- concentration increased from 0 to 5 mM. This could be ascribed to the fact that HCO_3^- is an effective scavenger for ·OH and $SO_4^{\bullet-}$, and $CO_3^{\bullet-}$, which generated in the reaction of HCO_3^- with ·OH/$SO_4^{\bullet-}$ radicals owns the weaker redox ability compared with ·OH/$SO_4^{\bullet-}$ radicals (Eqs. (13) and (14)) [53,54]. Thus, the decreased BPA degradation efficiency in this system could be due to the decreased number of ·OH / $SO_4^{\bullet-}$ radicals and the lower redox capacity of $CO_3^{\bullet-}$.

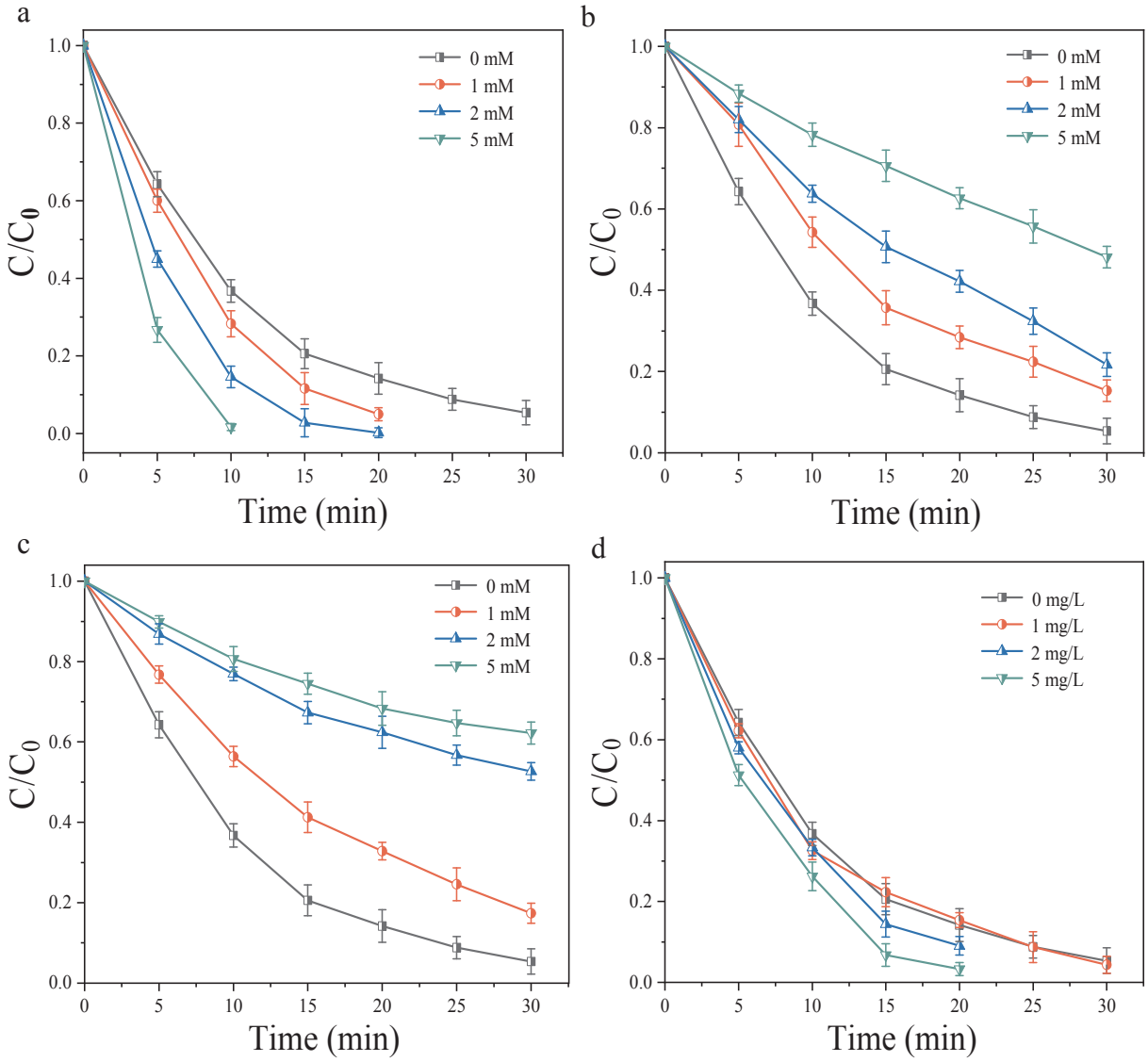

Fig. 9. Effects of Cl^- (a), HCO_3^- (b), $H_2PO_4^-$ (c), and HA (d) on BPA degradation in the TiO_2NTAs/PMS/VL system. Experimental conditions: [PMS] = 0.05 mM, [BPA] = 1 mg/L, [Cl^-] = [HCO_3^-] = [$H_2PO_4^-$] = 0–5 mM, [HA] = 0–5 mg/L, T = 25°C.

$$\cdot OH + HCO_3^- \rightarrow CO_3^{\cdot -} + H_2O \quad (13)$$

$$SO_4^{\cdot -} + HCO_3^- \rightarrow CO_3^{\cdot -} + HSO_4^- \quad (14)$$

As shown in Fig. 9c, the presence of phosphate would inhibit the BPA degradation in the TiO_2NTAs/PMS/VL system. The BPA removal efficiency was inhibited from 94.6% to 37.8% with the increase of phosphate from 0 to 5 mM. There were two probable reasons for this phenomenon. Firstly, phosphate anions might quench the active radicals in the reaction system as shown in Eqs. (15) and (16) [55,56]. Secondly, the previous study had found that the surface-adsorbed phosphates could effectively inhibit PMS sorption as well as its surface complexation on TiO_2 [28]. Due to the above two reasons, the BPA removal efficiency decreased when phosphate existed in the reaction system.

$$SO_4^{\cdot -} + H_2PO_4^- \rightarrow SO_4^{2-} + H_2PO_4^{\cdot} \quad (15)$$

$$\cdot OH + H_2PO_4^- \rightarrow OH^- + H_2PO_4^{\cdot} \quad (16)$$

As one of the main components of NOM, HA own a complex structures which may exert complicated influence on oxidation process. Therefore, it is necessary to investigate the effects of HA on BPA degradation in the TiO_2NTAs/PMS/VL system. As shown in Fig. 9d, the degradation rate of BPA was promoted after the addition of HA. With HA concentration increased from 0 to 5 mg L^{-1}, the degradation efficiency of BPA increased by 10.9% within 20 min. Generally, HA could compete with the pollutants for the ROS generated in the solution [57,58]. Besides, HA could also compete for photons with catalysts, resulting in the reduced generation of reactive species in the reaction system [59]. However, Cho et al. [60] found that as a photosensitizer, the excited HA by VL could eject electrons to the CB of TiO_2, and then degraded pollutants by a series of electron transfer processes. In this work, the enhanced photocatalytic performance might be due to the similar reason. Besides, as an electron acceptor, PMS could also combine with the electrons derived from the VL excited HA to generate corresponding reactive species. Since HA owns a complex chemical structures and properties, this issue deserves further studies.

3.8. Performance in actual water bodies

The drinking water and tap water were employed to investigate the performance of TiO_2NTAs/PMS/VL system in actual water bodies. The characteristics of drinking water and tap water were shown in Table S2.

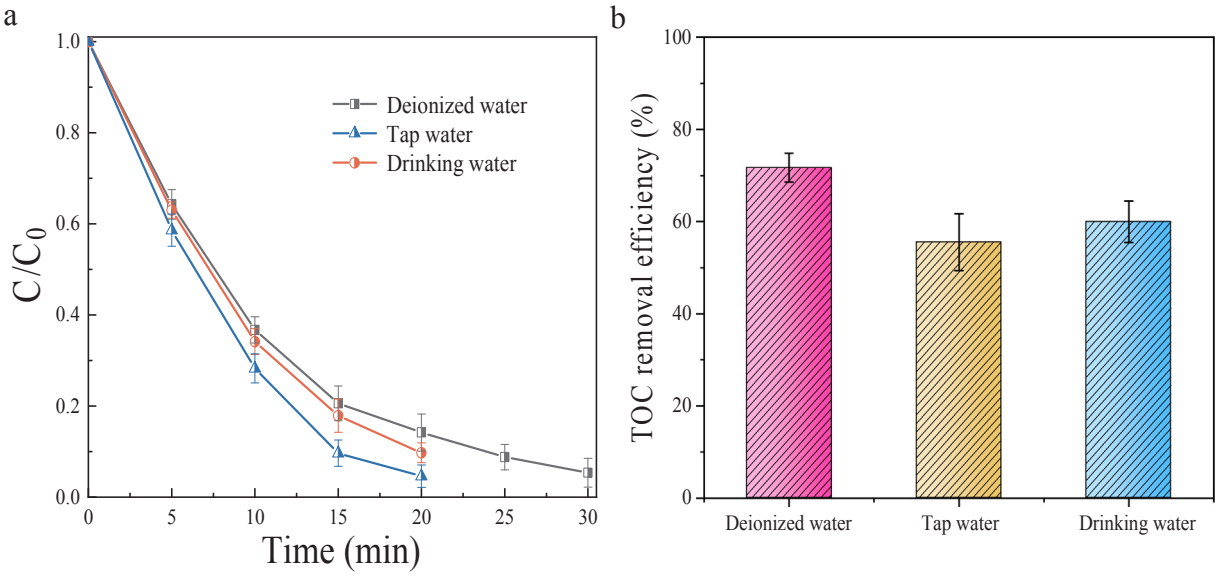

Fig. 10. The degradation efficiency of BPA in different water samples (a) and the corresponding TOC removal efficiency (b). Experimental conditions: [PMS] = 0.05 mM, [BPA] = 1 mg/L, T = 25℃.

As observed in Fig. 10a, the removal efficiency of BPA in deionized water was 85.8% within 20 min, while the degradation rates in drinking water and tap water were 90.3% and 95.4% during the same period, respectively. However, the TOC removal rate of deionized water (71.7%) was much higher than those of drinking water (60.0%) and tap water (55.5%) systems within 60 min (Fig. 10b). According to the characterization of drinking water and tap water (Table S2) and the results of section 3.6, it could be speculated that the Cl^- and/or some organic carbon in the water might promote the BPA degradation. However, the contrary in TOC mineralization was presumably correlated with the high TOC content. It was reported that some constituents of TOC could compete with BPA for radicals (e.g., ·OH and $SO_4^{\cdot -}$), thus restraining the mineralization of BPA [61]. Even so, the TOC removal efficiency in drinking water and tap water still remained above 55%. The high BPA and TOC removal efficiency in actual water bodies indicated the practicability of the TiO_2NTAs/PMS/VL system. It should be noted that although the use of sulfur-containing oxidants may lead to the release of sulfate anions to the environment, the dose of PMS in our study was only 0.05 mM, even if all of the PMS were converted to sulfate, the amount of sulfate was 4.8 mg/L, far less than the value specified in the Standards for drinking water quality in China (250 mg/L) [62], thus it could be deemed as a safe technology in practical application.

3.9. Stability of TiO_2NTAs

The stability of catalyst constitutes an important factor that determines the reusability of catalyst in practical engineering application. For this reason, the BPA degradation in TiO_2NTAs/PMS/VL system was repeated for 91 cycles to evaluate the long-term performance of TiO_2NTAs. As displayed in Fig. 11, the degradation efficiency of BPA decreased by about 10–12% after 30 tests. This might be ascribed to the adsorption of BPA and its degradation intermediates on TiO_2NTAs surface, which would weaken PMS complexation and activation. However, after ultrasonic treatment of the used TiO_2NTAs (conducted in 0.1 M H_2SO_4 solution for 1 min to clean the surface contaminants), the catalytic ability of TiO_2NTAs/PMS/VL system recovered to the previous level. Over 90 cycles, the degradation efficiency of BPA was still kept above 80%. Besides, after repeated use, the stability of TiO_2NTAs was investigated by the XRD and FT-IR characterizations. As shown in Fig. S5, the XRD pattern showed that the anatase of TiO_2

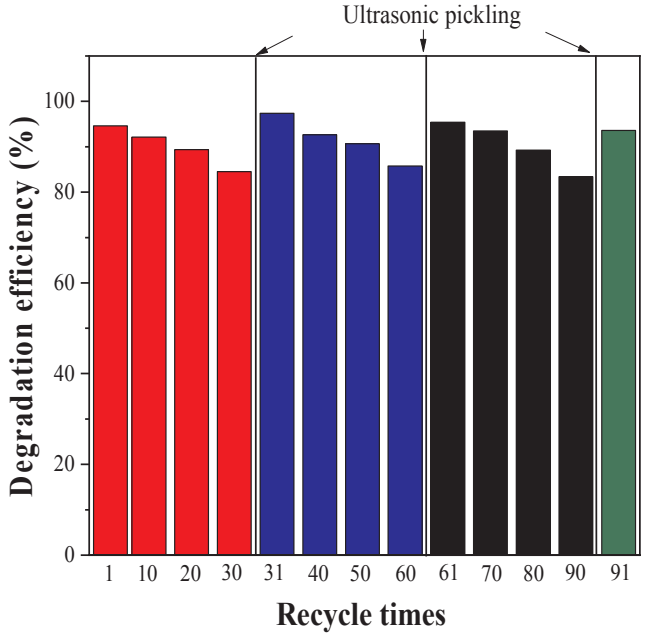

Fig. 11. Reusability test on the TiO_2NTAs/PMS/VL system for BPA degradation. Experimental Conditions: [PMS] = 0.05 mM, [BPA] = 1 mg/L, pH = 3.98, T = 25℃. Every recycle represents 30 min of reaction.

at 2θ 25.3° of the used TiO_2NTAs was still well crystalline after 90 recycles, meanwhile, the characteristic peak of Ti-O-Ti stretch at 580 cm^{-1} in the FT-IR spectrum was almost unchanged [63,64]. It should be noted that the –OH peak at around 3400 cm^{-1} in Fig. S5b was not observed, which might be attributed to that the repeated sample was dried in oven before testing. The above results demonstrated that TiO_2NTAs owned a fairly good stability and it could be used as a prospective candidate in PMS activation for pollutants degradation in practical application.

4. Conclusions

In this study, VL-induced photocatalytic activation of PMS at TiO_2NTAs was investigated. The results indicated that the combination

of TiO_2 with PMS under VL irradiation exhibited a synergistic effect for BPA removal. The quenching experiments and ESR measurements indicated that the $SO_4^{\bullet-}$ and ·OH were the main ROS for BPA degradation. By conducting a series of spectroscopic characterizations and photoelectrochemical measurements, the VL-responsive PMS-TiO_2 complex was proposed, which exhibited a lower band gap energy (2.61 eV) compared to the TiO_2NTAs (3.08 eV), and this complex could be induced by VL to inject electrons to activate PMS. In this process, PMS not only acted as a complexing agent, but also used as a radical precursor. The performance of TiO_2NTAs/PMS/VL system was better at acid and base conditions than that at neutral pH. The presence of Cl^- and HA obviously enhanced BPA degradation, while the addition of HCO_3^-, and $H_2PO_4^-$ exerted a negative effect on BPA degradation. The performances of long-term use of TiO_2NTAs and TiO_2NTAs/PMS/VL system in tap water and drinking water indicated that VL photocatalytic activation of PMS at TiO_2NTAs could serve as a feasible technology for remediation of contaminated tap water and drinking water.

CRediT authorship contribution statement

Jialin Jia: Conceptualization, Investigation, Data curation, Formal analysis, Validation, Writing - original draft, Writing - review & editing. **Dongmei Liu:** Writing - review & editing, Funding acquisition, Resources. **Songxue Wang:** Data curation, Methodology. **Huarui Li:** Data curation, Methodology. **Jiaxin Ni:** Data curation, Methodology. **Xiaobo Li:** Data curation, Methodology. **Jiayu Tian:** Writing - review & editing, Funding acquisition, Resources. **Qiao Wang:** Data curation, Methodology.

Declaration of Competing Interest

The authors declare that they have no known competing financial interests or personal relationships that could have appeared to influence the work reported in this paper.

Acknowledgments

This work was supported by the National Science Foundation of China (NO. 51978232 and 50808052), the State Key Laboratory of Urban Water Resource and Environment (HIT, 2021TS03), the Natural Science Foundation of Hebei Province (No. E2019202012), and the Natural Science Foundation of Tianjin (No. 19JCJQJC63000).

Appendix A. Supplementary material

Supplementary data to this article can be found online at https://doi.org/10.1016/j.seppur.2020.117510.

References

[1] X.J. Qiu, S.J. Y, M.W.L. Dzakpasu, X.P. Li, D.H. Ding, P.K. Jin, R.Z. Chen, Q.H. Zhang, X.C. Wang, Attenuation of BPA degradation by SO4•− in a system of peroxymonosulfate coupled with Mn/Fe MOF-templated catalysts and its synergism with Cl− and bicarbonate, Chem. Eng. J., 372 (2019), pp. 605–615.
[2] M. Dietrich, M. Franke, M. Stelter, P. Braeutigam, Degradation of endocrine disruptor bisphenol A by ultrasound-assisted electrochemical oxidation in water, Ultrason. Sonochem. 39 (2017) 741–749.
[3] D. Wu, L. He, R.N. Sun, M.P. Tong, H.J. Kim, Influence of bisphenol A on the transport and deposition behaviors of bacteria in quartz sand, Water Res. 121 (2017) 1–10.
[4] H. Fukazawa, K. Hoshino, T. Shiozawa, H. Matsushita, Y. Terao, Identification and quantification of chlorinated bisphenol A in wastewater from wastepaper recycling plants, Chemosphere 44 (2001) 973–979.
[5] F. Wang, J. Yao, K. Sun, B.S. Xing, Adsorption of dialkyl phthalate esters on carbon nanotubes, Environ. Sci. Technol. 44 (2010) 6985–6991.
[6] C. Loderer, A. Wörle, W. Fuchs, Influence of different mesh filter module configurations on effluent quality and long-term filtration performance, Environ. Sci. Technol. 46 (2012) 3844–3850.
[7] V.J.P. Vilar, F.C. Moreira, A.C.C. Ferreira, M.A. Sousa, C. Gonçalves, M.F. Alpendurada, R.A.R Boaventura, Biodegradability enhancement of a pesticide-containing bio-treated wastewater using a solar photo-Fenton treatment step followed by a biological oxidation process, Water Res. 46 (2012) 4599–4613.
[8] J. Deng, Y.J. Ge, C.Q. Tan, H.Y. Wang, Q.S. Li, S.Q. Zhou, K.J. Zhang, Degradation of ciprofloxacin using α-MnO_2 activated peroxymonosulfate process: effect of water constituents, degradation intermediates and toxicity evaluation, Chem. Eng. J. 330 (2017) 1390–1400.
[9] Y.X. Liu, Z.Y. Liu, Y. Wang, Y.S. Yin, J.F. Pan, J. Zhang, Q. Wang, Simultaneous abosrption of SO_2 and NO from flue gas using ultrasound/Fe^{2+}/heat coactivated persulfate system, J. Hazard. Mater. 342 (2018) 326–334.
[10] W.H. Chu, D.M. Li, N.Y. Gao, M.R. Templeton, C.Q. Tan, Y.Q. Gao, The control of emerging haloacetamide DBP precursors with UV/persulfate treatment, Water Res. 72 (2015) 340–348.
[11] W.H. Chu, J.L. Hu, T. Bond, N.Y. Gao, B. Xu, D.Q. Yin, Water temperature significantly impacts the formation of iodinated haloacetamides during persulfate oxidation, Water Res. 98 (2016) 47–55.
[12] C.D. Qi, X.T. Liu, J. Ma, C.Y. Lin, X.W. Li, H.J. Zhang, Activation of peroxymonosulfate by base: implications for the degradation of organic pollutants, Chemosphere 151 (2016) 280–288.
[13] F. Ghanbari, M. Moradi, Application of peroxymonosulfate and its activation methods for degradation of environmental organic pollutants, Review Chem. Eng. J. 310 (1) (2017) 41–62.
[14] J.L. Wang, S.Z. Wang, Activation of persulfate (PS) and peroxymonosulfate (PMS) and application for the degradation of emerging contaminants, Chem. Eng. J. 334 (2018) 1502–1517.
[15] R.R. Solís, F.J. Rivas, M. Tierno, Monopersulfate photocatalysis under 365 nm radiation. Direct oxidation and monopersulfate promoted photocatalysis of the herbicide tembotrione, J. Environ. Manage. 181 (2016) 385–394.
[16] Y. Zhou, J. Jiang, Y. Gao, S.Y. Pang, Y. Yang, J. Ma, J. Gu, J. Li, Z. Wang, L.H. Wang, L.P. Yuan, Y. Yang, Activation of peroxymonosulfate by phenols: important role of quinone intermediates and involvement of singlet oxygen, Water Res. 125 (2017) 209–218.
[17] R.J. Watts, M. Ahmad, A.K. Hohner, A.L. Teel, Persulfate activation by glucose for in situ chemical oxidation, Water Res. 133 (2018) 247–254.
[18] S.Q. Zhou, Y.H. Yu, W.Q. Zhang, X.Y. Meng, J.M. Luo, L. Deng, Z. Shi, C. Crittenden, Oxidation of microcystin-LR via activation of peroxymonosulfate using ascorbic acid: kinetic modeling and toxicity assessment, Environ. Sci. Technol. 52 (7) (2018) 4305–4312.
[19] M. Andersson, L. Osterlund, S. Ljungstrom, A. Palmqvist, Preparation of nanosize anatase and rutile TiO_2 by hydrothermal treatment of microemulsions and their activity for photocatalytic wet oxidation of phenol, J. Phys. Chem. B. 106 (2002) 10674–10679.
[20] S. Malato, J. Blanco, C. Richter, B. Braun, M.I. Maldonado, Enhancement of the rate of solar photocatalytic mineralization of organic pollutants by inorganic oxidizing species, Appl. Catal. B: Environ. 17 (1998) 347–356.
[21] B.T. Xu, M.B. Ahmed, J.L. Zhou, A. Altaee, Visible and UV photocatalysis of aqueous perfluorooctanoic acid by TiO_2 and peroxymonosulfate: process kinetics and mechanistic insights, Chemosphere 243 (2020) 125366.
[22] X.Y. Chen, W.P. Wang, H. Xiao, C.L. Hong, F.X. Zhu, Y.L. Yao, Z.Y. Xue, Accelerated TiO_2 photocatalytic degradation of Acid Orange 7 under visible light mediated by peroxymonosulfate, Chem. Eng. J. 193–194 (2012) 290–295.
[23] G. Zhang, G. Kim, W.Y. Choi, Visible light driven photocatalysis mediated via ligand to-metal charge transfer (LMCT): an alternative approach to solar activation of titania, Energy Environ. Sci. 7 (2014) 954–966.
[24] W.S. Ang, S. Lee, Elimelech, M, Chemical and physical aspects of cleaning of organic-fouled reverse osmosis membranes, J. Membr. Sci. 272 (1–2) (2006) 198–210.
[25] D. Li, J.L. Jia, T. Zheng, X.W. Cheng, X.J. Yu, Construction and characterization of visible light active Pd nano-crystallite decorated and C-N-S-co-doped TiO_2 nanosheet array photoelectrode for enhanced photocatalytic degradation of acetylsalicylic acid, Chem. Eng. J. 279 (2015) 264–272.
[26] G.S. Liu, Y.N. Zhou, J. Teng, J.N. Zhang, S.J. You, Visible-light-driven photocatalytic activation of peroxymonosulfate by $Cu_2(OH)PO_4$ for effective decontamination, Chemosphere 201 (2018) 197–205.
[27] S. Kim, W.Y. Choi, Visible-light-induced photocatalytic degradation of 4-chlorophenol and phenolic compounds in aqueous suspension of pure titania: demonstrating the existence of a surface-complex-mediated path, J. Phys. Chem. B. 109 (2005) 5143–5149.
[28] Y.S. Jo, C.Y. Kim, G.H. M, J.S. Lee, T.C. An, W.Y. Choi, Activation of peroxymonosulfate on visible light irradiated TiO2 via a charge transfer complex path, Chem. Eng. J., 346 (2018), pp. 249–257.
[29] G. Colón, M.C. Hidalgo, G. Munuera, I. Ferino, M.G. Cutrufello, J.A. Navı´o, Structural and surface approach to the enhanced photocatalytic activity of sulfated TiO2 photocatalyst, Appl. Catal. B: Environ., 63 (2006), pp. 45–59.
[30] G. Ahmed, M. Hanif, L.Z. Zhao, M. Hussain, J. Khan, Z.W. Liu, Defect engineering of ZnO nanoparticles by graphene oxide leading to enhanced visible light photocatalysis, J. Mol. Catal. A: Chem. 425 (2016) 310–321.
[31] J. Gonzalez, M. Torrent-Sucarrat, J.M. Anglada, The reactions of SO_3 with HO_2 radical and H_2O-HO_2 radical complex. Theoretical study on the atmospheric formation of HSO_5 and H_2SO_4, Phys. Chem. Chem. Phys. 12 (2010) 2116–2125.
[32] Q. Wang, Z.Q. Liu, D.M. Liu, G.S. Liu, M. Yang, F.Y. Cui, W. Wang, Ultrathin two-dimensional $BiOBr_xI_{1-x}$ solid solution with rich oxygen vacancies for enhanced visible-light-driven photoactivity in environmental remediation, Appl. Catal. B: Environ. 236 (2018) 222–232.
[33] H.T. Yu, J. Ma, Y.X. Zhang, X.J. Zhang, W.T. Shi, Cyclic voltammetry studies of TiO_2 nanotube arrays electrode: Conductivity and reactivity in the presence of H^+ and aqueous redox systems, Electrochim. Acta. 56 (2011) 6498–6502.

[34] Z.G. Zhu, C.H. Ji, L.L. Zhong, S. Liu, F.Y. Cui, H.L. Sun, W. Wang, Magnetic Fe–Co crystal doped hierarchical porous carbon fibers for removal of organic pollutants, J. Mater. Chem. A. 5 (2017) 18071–18080.
[35] E. Saputra, S. Muhammad, H.Q. Sun, H.-M. Ang, M.O. Tadé, S.B. Wang, Shape-controlled activation of peroxymonosulfate by single crystal α-Mn_2O_3 for catalytic phenol degradation in aqueous solution, Appl. Catal. B: Environ. 154–155 (2014) 246–251.
[36] Y.X. Wang, H.Q. Sun, H.M. Ang, M.O. Tadé, S.B. Wang, Magnetic Fe_3O_4/carbon sphere/cobalt composites for catalytic oxidation of phenol solutions with sulfate radicals, Chem. Eng. J. 245 (2014) 1–9.
[37] H.R. Song, L.X. Yan, Y.W. Wang, J. Jiang, J. Ma, C.P. Li, G. Wang, J. Gu, P. Liu, Electrochemically activated PMS and PDS: Radical oxidation versus nonradical oxidation, Chem. Eng. J. 391 (2020) 123560.
[38] Y. Xie, P. Li, Y. Zeng, X. Li, Y. Xiao, Y. Wang, Y. Zhang, Thermally treated fungal manganese oxides for bisphenol A degradation using sulfate radicals, Chem. Eng. J. 335 (2018) 728–736.
[39] X.B. Dong, B.X. Ren, Z.M. Sun, C.Q. Li, X.W. Zhang, M.H. Kong, S.L. Zheng, D.D. Dionysiou, Monodispersed $CuFe_2O_4$ nanoparticles anchored on natural kaolinite as highly efficient peroxymonosulfate catalyst for bisphenol A degradation, Appl. Catal. B: Environ. 253 (2019) 206–217.
[40] L. Xu, L. Yang, E.M.J. Johansson, Y. Wang, P. Jin, Photocatalytic activity and mechanism of bisphenol a removal over TiO_2-x/rGO nanocomposite driven by visible light, Chem. Eng. J. 350 (2018) 1043–1055.
[41] Y. Zhang, N. Qin, J. Li, S. Han, P. Li, G. Zhao, Facet exposure-dependent photoelectrocatalytic oxidation kinetics of bisphenol A on nanocrystalline 001 TiO2/carbon aerogel electrode, Appl. Catal. B: Environ. 216 (2017) 30–40.
[42] L.W. Chen, X. Zuo, L. Zhou, Y. Huang, S.J. Yang, T.M. Cai, D.H. Ding, Efficient heterogeneous activation of peroxymonosulfate by facilely prepared Co/Fe bimetallic oxides: kinetics and mechanism, Chem. Eng. J. 345 (2018) 364–374.
[43] R.X. Yuan, L. Hu, P. Yu, H.Y. Wang, Z.H. Wang, J.Y. Fang, Nanostructured Co_3O_4 grown on nickel foam: an efficient and readily recyclable 3D catalyst for heterogeneous peroxymonosulfate activation, Chemosphere 198 (2018) 204–215.
[44] S.D. Yan, J.Y. Geng, R. Guo, Y. Du, H. Zhang, Hydronium jarosite activation of peroxymonosulfate for the oxidation of organic contaminant in an electrochemical reactor driven by microbial fuel cell, J. Hazard. Mater. 333 (2017) 358–368.
[45] M.M. Halmann, Photodegradation of Water Pollutants, CRC Press, New York, USA, 1996.
[46] H. Elias, U. Gotz, K.J. Wannowius, Kinetics and mechanism of the oxidation of sulfur(Iv) by peroxomonosulfuric acid anion, Atmos Environ. 28 (1994) 439–448.
[47] X.G. Duan, C. Su, L. Zhou, H.Q. Sun, A. Suvorova, T. Odedairo, Z.H. Zhu, Z.P. Shao, S.B. Wang, Surface controlled generation of reactive radicals from persulfate by carbocatalysis on nanodiamonds Appl. Catal. B: Environ., 194 (2016) 7–15.
[48] R.R. Solísa, I.F. Mena, M.N. Nadagouda, D.D. Dionysiou, Adsorptive interaction of peroxymonosulfate with graphene and catalytic assessment via non-radical pathway for the removal of aqueous pharmaceuticals, J. Hazard Mater. 384 (2020) 121340.
[49] Y. Guo, T. Shen, C. Wang, J. Sun, X. Wang, Rapid removal of caffeine in aqueous solutions by peroxymonosulfate oxidant activated with cobalt ion, Water. Sci. Technol. 72 (2015) 478.
[50] W.D. Oh, S.K. Lua, Z. Dong, T.T. Lim, Performance of magnetic activated carbon composite as peroxymonosulfate activator and regenerable adsorbent via sulfate radical-mediated oxidation processes, J. Hazard Mater. 284 (2015) 1–9.
[51] G.P. Anipsitakis, T.P. Tufano, D.D. Dionysiou, Chemical and microbial decontamination of pool water using activated potassium peroxymonosulfate, Water Res. 42 (2008) 2899–2910.
[52] C. Liang, Z.S. Wang, N. Mohanty, Influences of carbonate and chloride ions on persulfate oxidation of trichloroethylene at 20 degrees C, Sci. Total Environ. 370 (2006) 271–277.
[53] E. Robert, C.L. Huie Clifton, Temperature dependence of the rate constants for reactions of the sulfate radical, SO_4, with anions, Am. Chem. Soc. 94 (1990) 8561–8567.
[54] A. Ghauch, A.M. Tuqan, Oxidation of bisoprolol in heated persulfate/H_2O systems: kinetics and products, Chem. Eng. J. 183 (2012) 162–171.
[55] P.D. Hu, M.C. Long, Cobalt-catalyzed sulfate radical-based advanced oxidation: a review on heterogeneous catalysts and applications, Appl. Catal. B: Environ. 181 (2016) 103–117.
[56] F. Qi, W. Chu, B.B. Xu, Modeling the heterogeneous peroxymonosulfate/Co-MCM41 process for the degradation of caffeine and the study of influence of cobalt sources, Chem. Eng. J. 235 (2014) 10–18.
[57] Y.L. Song, J.Y. Tian, S.S. Gao, P.H. Shao, J.Y. Qi, F.Y. Cui, Photodegradation of sulfonamides by g-C_3N_4 under visible light irradiation: effectiveness, mechanism and pathways, Appl. Catal. B: Environ. 210 (2017) 88–96.
[58] S.X. Wang, J.Y. Tian, Q. Wang, F. Xiao, S.S. Gao, W.X. Shi, F.Y. Cui, Development of CuO coated ceramic hollow fiber membrane for peroxymonosulfate activation: a highly efficient singlet oxygen-dominated oxidation process for bisphenol a degradation, Appl. Catal. B: Environ. 256 (2019) 117783.
[59] K.H. Chan, W. Chu, Effect of humic acid on the photolysis of the pesticide atrazine in a surfactant-aided soil-washing system in acidic condition, Water Res. 39 (2005) 2154–2166.
[60] Y.M. Cho, W.Y. Choi, Visible light-induced reactions of humic acids on TiO_2, J. Photochem. Photobiol. A. 148 (2002) 129–135.
[61] L.M. Hu, G.S. Zhang, M. Liu, Q. Wang, P. Wang, Enhanced degradation of Bisphenol A (BPA) by peroxymonosulfate with Co3O4-Bi2O3 catalyst activation: Effects of pH, inorganic anions, and water matrix, Chem. Eng. J., 338 (2018), pp. 300–310.
[62] ⟨⟨Standards for drinking water quality⟩⟩ (GB 5749-2006).
[63] D. Li, J.L. Jia, Y.H. Zhang, N. Wang, X.L. Guo, X.J. Yu, Preparation and characterization of Nano-graphite/TiO_2 composite photoelectrode for photoelectrocatalytic degradation of hazardous pollutant, J. Hazard Mater. 315 (2016) 1–10.
[64] J.F. Shen, B. Yan, M. Shi, H.W. Ma, N. Li, M.X. Ye, One step hydrothermal synthesis of TiO_2-reduced graphene oxide sheets, J. Mater. Chem. 21 (2011) 3415.